Stratosphere-to-troposphere transport revealed by ground-based lidar and ozonesonde at a midlatitude site

Shi Kuang,[1] M. J. Newchurch,[1] John Burris,[2] Lihua Wang,[1] Kevin Knupp,[1] and Guanyu Huang[1]

Received 27 February 2012; revised 3 August 2012; accepted 14 August 2012; published 21 September 2012.

[1] This paper presents ozone structures measured by a ground-based ozone lidar and ozonesonde at Huntsville, Alabama, on 27–29 April 2010 originating from a stratosphere-to-troposphere transport event associated with a cutoff cyclone and tropopause fold. In this case, the tropopause reached 6 km and the stratospheric intrusion resulted in a 2-km thick elevated ozone layer with values between 70 and 85 ppbv descending from the ~306-K to 298-K isentropic surface at a rate of ~5 km day^{-1}. The potential temperature was provided by a collocated microwave profiling radiometer. We examine the corresponding meteorological fields and potential vorticity (PV) structures derived from the analysis data from the North American Mesoscale model. The 2-PVU (PV unit) surface, defined as the dynamic tropopause, is able to capture the variations of the ozone tropopause estimated from the ozonesonde and lidar measurements. The estimated ozone/PV ratio, from the measured ozone and model derived PV, for the mixing layer between the troposphere and stratosphere is ~41 ppbv/PVU with an uncertainty of ~33%. Within two days, the estimated mass of ozone irreversibly transported from the stratospheric into the troposphere is between 0.07 Tg (0.9×10^{33} molecules) and 0.11 Tg (1.3×10^{33} molecules) with an estimated uncertainty of 59%. Tropospheric ozone exhibited enormous variability due to the complicated mixing processes. Low ozone and large variability were observed in the mid-troposphere after the stratospheric intrusion due to the westerly advection including the transition from a cyclonic system to an anticyclonic system. This study using high temporal and vertical-resolution measurements suggests that, in this case, stratospheric air quickly lost its stratospheric characteristics once it is irreversibly mixed down into the troposphere.

Citation: Kuang, S., M. J. Newchurch, J. Burris, L. Wang, K. Knupp, and G. Huang (2012), Stratosphere-to-troposphere transport revealed by ground-based lidar and ozonesonde at a midlatitude site, *J. Geophys. Res.*, *117*, D18305, doi:10.1029/2012JD017695.

1. Introduction

[2] When viewed from a global-scale perspective, stratosphere-troposphere exchange (STE) is driven by the Brewer-Dobson circulation with upward motion across the tropopause at the equator and downward motion in the extratropics. These fluxes, which partly govern the global chemical transport, significantly affect the radiative forcing associated with global climate change (for review, see *Holton et al.* [1995] and *Stohl et al.* [2003a]).

[3] The identification of the tropopause is important because it significantly affects the quantification of the cross-tropopause air mass flux. Depending on different applications, there are at least three conventional tropopause definitions: thermal tropopause, based on temperature lapse rate [*World Meteorological Organization* (*WMO*), 1986]; chemical tropopause, based on trace gas (e.g., ozone, CO) concentration [*Browell et al.*, 1996], gradient, or both [*Bethan et al.*, 1996]; and dynamic tropopause, based on certain threshold of potential vorticity (PV) [*Holton et al.*, 1995]. The *WMO* [1986] defines the tropopause as the lowest level at which the lapse rate decrease to 2 K km^{-1} or less, and the lapse rates within the 2-km thick layer from this level do not exceed 2 K km^{-1}. The thermal tropopause is popular because it represents the chemical transition layer very well in the extratropics [*Pan et al.*, 2004], and can also be easily calculated with a sounding or model temperature profile. The dynamic tropopause has an advantage in quantifying the conservative transport across the tropopause [*Dethof et al.*, 2000] when it is treated as a material surface. 1.6, 2, or 3.5 PV unit (PVU = 10^{-6} K m^2 kg^{-1} s^{-1}) is often chosen as the threshold [*Hoerling et al.*, 1991; *Hoinka*, 1998; *Wernli and Bourqui*, 2002]. PV is widely used as a stratospheric tracer

[1]Atmospheric Science Department, University of Alabama in Huntsville, Huntsville, Alabama, USA.
[2]NASA Goddard Space Flight Center, Greenbelt, Maryland, USA.

Corresponding author: S. Kuang, Atmospheric Science Department, University of Alabama in Huntsville, 320 Sparkman Dr., Huntsville, AL 35805, USA. (kuang@nsstc.uah.edu)

to investigate the influence of cross-tropopause exchange on the troposphere [*James et al.*, 2003; *Wernli and Bourqui*, 2002]. There is no standard criterion to define the chemical tropopause because both the concentration and gradient of trace gases at the tropopause vary widely with location and season. However, some definitions of chemical tropopause are popular, such as *Bethan et al.*'s [1996] ozone tropopause criterion which defines the tropopause as the altitude at which the ozone mixing ratio is greater than 80 ppbv, ozone gradient exceeds 60 ppbv/km in a depth of 200 m, and the ozone above the tropopause exceeds 110 ppbv. Another definition by *Pan et al.*'s [2004] identifies the chemical tropopause at the intersection point of a stratospheric tracer (e.g., ozone) increasing and a tropospheric tracer (e.g., water vapor) decreasing with altitude. In this paper, we employ the tropopause heights calculated using all three of the above definitions and data from either local observations or model calculations.

[4] Stratosphere-to-troposphere transport (STT) (i.e., stratospheric intrusion), which hereafter refers to only downward motion of the STE, makes an important contribution (at least 10%) to the budget of tropospheric ozone [*Fusco and Logan*, 2003; *Lelieveld and Dentener*, 2000; *Thompson et al.*, 2007] although the debate about its quantitative significance continues. In North America, STT occurs mostly frequently in the midlatitudes between 40°N and 65°N, however, its impact is mostly confined to the subtropical lower troposphere (maximized at 30–40°N) [*Hsu et al.*, 2005; *Wernli and Bourqui*, 2002] due to quasi-isentropic descent. Deep STT events are often found in the midlatitude storm track regions associated with baroclinic activities, such as tropopause folding and cutoff cyclones, and account for ~15% of the total STT mass flux during winter according to the model study by *Wernli and Bourqui* [2002]. Most of the STT contributes to the tropospheric budget through a shallow and transient exchange [*James et al.*, 2003]. However, those deep STT events significantly change the oxidizing capacity of the troposphere and even enhance the surface maxima [*Langford et al.*, 2009; *Lefohn et al.*, 2011]. In terms of the seasonal cycle, the maximum net downward cross tropopause transport of ozone occurs in spring [*Hsu et al.*, 2005; *Olsen et al.*, 2004] despite the comparable net downward air mass flux in winter and spring [*Wernli and Bourqui*, 2002]. STT plays a considerably important role for the spring maximum of the background ozone in the North Hemisphere [*Monks*, 2000; *Stohl et al.*, 2003b], which is defined as the ozone not attributed to anthropogenic sources of local origin, although the dominant factor is believed to be local photochemical production [*Vingarzan*, 2004].

[5] Several mechanisms have been associated with STTs including tropopause folding [*Danielsen*, 1968; *Shapiro*, 1980], cutoff cyclones [*Gouget et al.*, 2000; *Langford et al.*, 1996; *Price and Vaughan*, 1993; *Vaughan et al.*, 1994], and gravity wave breaking [*Lamarque et al.*, 1996]. Both cutoff cyclones and tropopause folds are often found together, with the former emphasizing the horizontal distribution of weather systems and the latter emphasizing vertical structure. A cutoff cyclone/low is a cyclonic circulation in the geopotential height field in the middle or upper troposphere isolated from the main trough in the westerlies. Climatically, cutoff cyclones occur more frequently in summer (50%) and spring (30%) [*Nieto et al.*, 2005]. The lifetimes of cutoff cyclones are usually 2–3 days. Notwithstanding the highly variable estimations of the ozone flux due to cutoff cyclones in the previous studies, they make a major contribution to tropospheric ozone budgets [*Ancellet et al.*, 1991].

[6] Lidars have long been used to measure STT structures [*Browell et al.*, 1987; *Eisele et al.*, 1999] and STT contributions to the tropospheric-ozone abundance [*Ancellet et al.*, 1991; *Vaughan et al.*, 1994]. Because of its high resolution and continuous observational capability, a lidar is the ideal instrument to capture rapid variations in ozone distribution. Lidar observations can validate various atmospheric models [*Zanis et al.*, 2003], particularly where high spatial and temporal resolution are required, and improve our understanding of the ozone budget. Although STT observations are extensively discussed in the literature, observations of intrusions south of 35°N are not reported frequently. This paper will present and analyze the lidar and ozonesonde measurements made over Huntsville associated with an STT event, estimate its flux into the troposphere, and discuss the resulting tropospheric ozone variability.

2. Instrumentation

2.1. Lidar

[7] Located in the Regional Atmospheric Profiling Center for Discovery (RAPCD) on the campus of the University of Alabama in Huntsville (UAHuntsville) (34.72°N, 86.65°W, 206-m asl), the ozone Differential Absorption Lidar (DIAL) makes retrievals from 0.5 to ~12 km above ground level (AGL) during both daytime and nighttime with a typical temporal resolution of 10 min and range resolution of 750 m. This system operates with two wavelengths, 285 and 291 nm, and employs two receivers, one 10-cm in diameter and the second 40 cm. Recent transmitter upgrades have extended the upper observation limit from ~8 to ~12 km and the addition of a third photomultiplier (PMT) channel has extended the lower retrieval from 1 to 0.5 km AGL. An iterative aerosol correction [*Kuang et al.*, 2011a] is applied to reduce errors arising from differential aerosol backscattering typically encountered below 6 km. Validation of the lidar measurements using ozonesondes has shown that the uncertainties for a 10-min retrieval are less than 10% below 4 km AGL and less than 20% below 8 km [*Kuang et al.*, 2011a]. Generally, signals contaminated by clouds below 3 km are automatically discarded by the software. Higher altitude cloud interference is removed manually.

2.2. Ozonesonde

[8] The Huntsville ozonesonde station is a joint effort between the Earth System Science Center of the UAHuntsville and the NOAA's Global Monitoring Division (formerly Climate Monitoring and Diagnostic Laboratory) in the Earth System Research Laboratory. Weekly ozonesonde (ENSCI model 2Z) observations have been made in Huntsville since 1999 [*Newchurch et al.*, 2003] and have been used to validate the DIAL measurements. The ozonesondes used in Huntsville employ an Electrochemical Concentration Cell (ECC) sensor [*Komhyr*, 1969], with 2% unbuffered potassium iodide (KI) cathode solution, to measure ozone partial pressure, and a Vaisala RS-80 radiosonde to measure, ambient temperature, pressure, and dew point up to 35 km altitude. This ECC-type ozonesonde is currently the most widely used

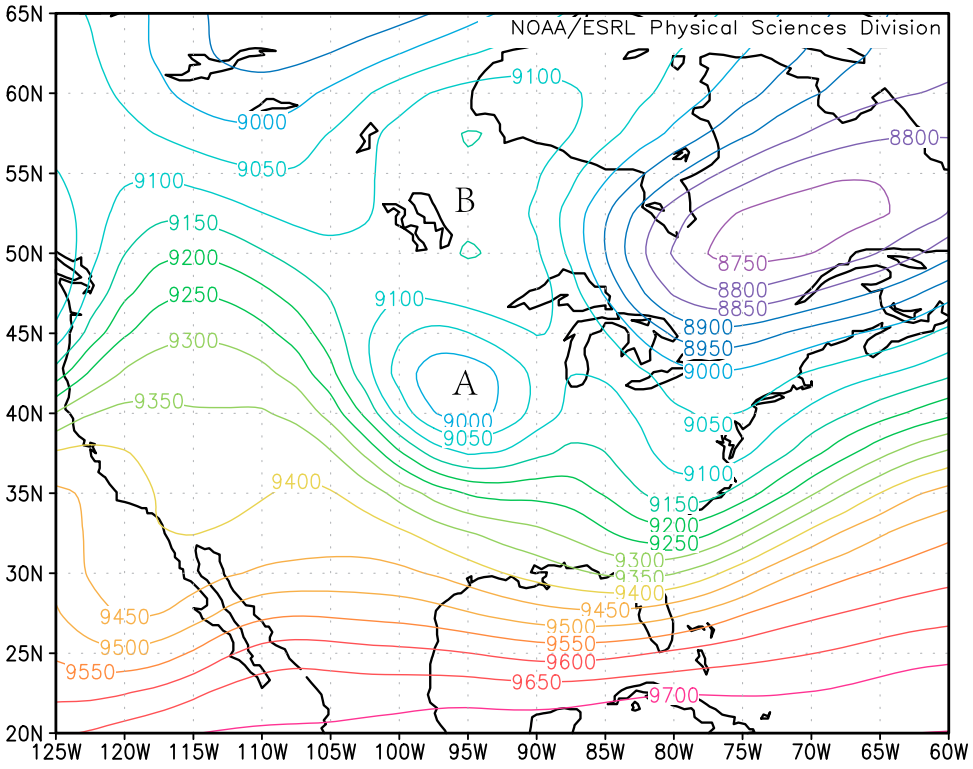

Figure 1. NOAA/NCEP 300-hPa heights for 0000 UTC 27 April 2010 showing the cutoff cyclone (A) and blocking high (B) (source: Physical Sciences Division of Earth System Research Laboratory of NOAA, http://www.esrl.noaa.gov/psd/).

instrument to measure the vertical tropospheric ozone profiles due to its well-characterized behavior and working capability under various sky conditions. The typical ascent rate of the balloon-borne ozonesondes is ~5 m/s and the response time of the sensor to a step change in ozone concentration is ~20–30 s [*Komhyr et al.*, 1995; *Smit et al.*, 2007] meaning that the vertical resolution of the ozonesonde measurements is approximately 100–150 m. Recent assessment experiments suggest that the ENSCI 2Z ozonesondes measure ozone with a precision better than ±5% and a accuracy better than ±10% up to 30 km if the sondes are prepared and operated properly, although there exist systematic biases less than 7% with different sensing solution and manufacture years [*Johnson et al.*, 2002, 2008; *Smit et al.*, 2007].

2.3. MPR

[9] The potential temperature (Θ) used in this paper is provided by a collocated microwave profiling radiometer (MPR, Radiometrics TP/WVP-3000) [*Ware et al.*, 2003]. Although this paper will present only temperature measurements, the MPR measures temperature and water vapor density up to 10 km height with seven discrete frequency bands from 51 to 59 GHz and five bands from 22 to 30 GHz [*Solheim et al.*, 1998], respectively. The MPR reports temperature retrievals every 100 m below 1 km and every 250 m from 1 to 10 km with a temporal resolution of 1 min, and uncertainty of ~2 K [*Güldner and Spänkuch*, 2001]. The vertical resolution decreases from ~100 m below 1.2 km to ~1 km at 10 km. Extensive applications of the MPR on severe weather and atmospheric chemistry in UAHuntsville have been reported by *Knupp* [2006], *Knupp et al.* [2009], *Karan and Knupp* [2006], and *Kuang et al.* [2011b].

3. Results

3.1. Meteorological Analysis

[10] As shown on the 300-hPa upper-air chart for 0000 UTC 27 April 2010 in Figure 1 (thereafter all times refer to UTC), a cutoff cyclone centered above Illinois (about 95°W, 40°N) separated from the main cyclone centered above Quebec due to a blocking anticyclone above Manitoba, Canada. This cutoff cyclone developed on 26 April and merged back to the main trough on 28 April with a two-day lifetime. For further analysis, we examine the meteorological fields from the North American Mesoscale (NAM) model from the National Centers for Environmental Prediction (NCEP) [*Janjic*, 2003]. The NAM outputs have a horizontal resolution of ~13 km and 39 vertical pressure layers from 1000 to 50 hPa. Figure 2a shows the horizontal distributions of 300-hPa wind speed and RH for 1200 27 April (12 h later than the time for Figure 1). The 300-hPa surface is helpful for STT diagnostics because it is usually the highest tropospheric layer in the extratropics with good STT detection sensitivity. Both the main and cutoff cyclones have corresponding low humidity regions. The hook-shaped low water vapor stream outlines the region containing dry stratospheric air 'leaked' into the troposphere. The jet stream, which is often found concurrent with a stratospheric intrusion [*Ravetta et al.*, 1999; *Sorensen and Nielsen*, 2001], was

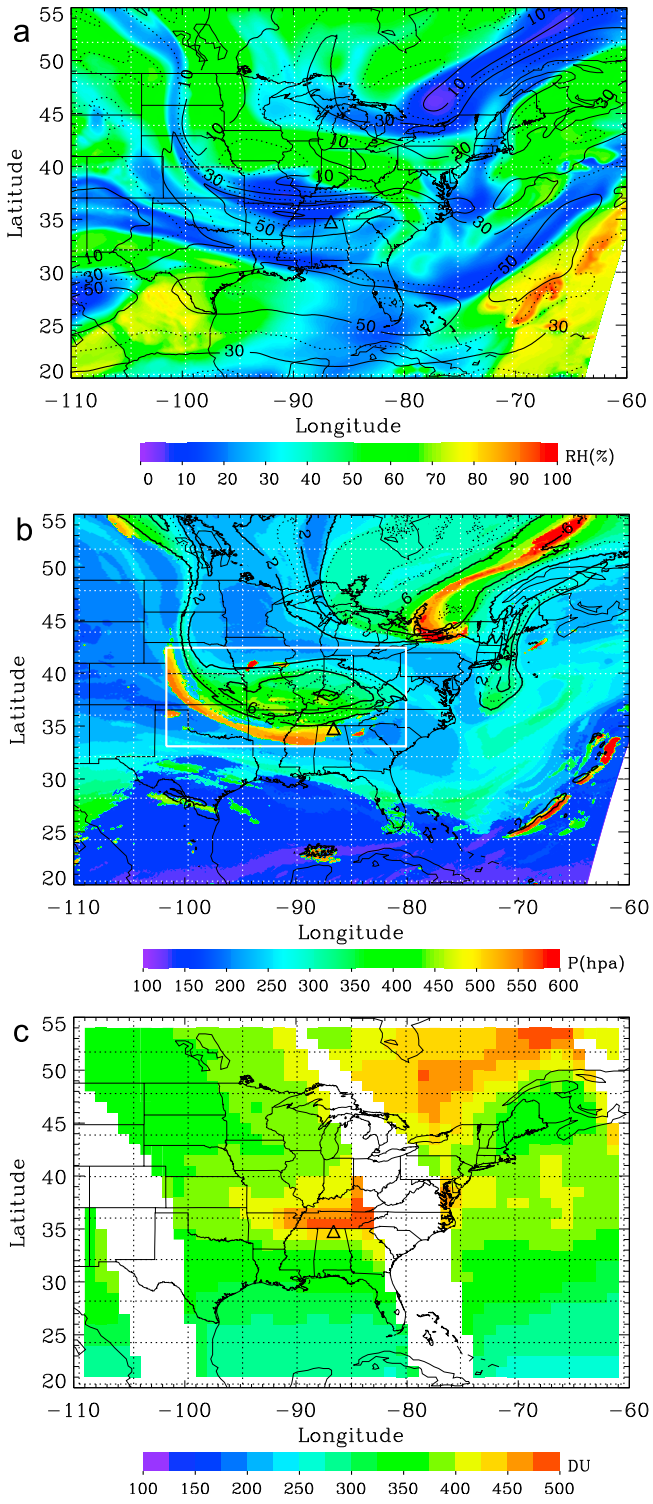

Figure 2. Horizontal distributions of (a) wind speed (solid black lines) and RH (colors) at 300 hPa of NAM at 1200 UTC (the lidar location is marked by the black triangle). (b) IPV (black lines) at 320-K isentropic surface with a 2-PVU interval and the lowest 2-PVU surface pressure (colors) at 1200 UTC derived from NAM. (c) OMI total ozone, on 27 April 2010. The white square in Figure 2b marks the spatial area for the STT ozone budget calculation in section 3.4.

located just above Huntsville with a maximum wind speed exceeding 60 m/s. The wind speed at the main cyclone was less than 20 m/s and much weaker than at the cutoff low.

[11] Figure 2b presents the 320-K isentropic potential vorticity (IPV), denoted by the black lines, and lowest 2-PVU surface pressure, represented by colors, for investigation of the stratospheric intrusion depth and estimation of the ozone budget of irreversible mixing. For this particular tropopause folding case, the 2-PVU dynamic tropopause is more appropriately seen as a lowest layer of the air originating from STT rather than the material distinction of the troposphere and stratosphere. The stratospheric- intrusion air may be located in the upper troposphere without losing the characteristics of stratospheric air. By using PV as a stratospheric tracer, we show how and where the ozone above the 2-PVU surface is permanently mixed down into the troposphere. On the 320-K Θ surface, the shape of the PV anomaly associated with the cutoff low, centered at (~38°N, ~90°W), agrees well with the dry air region shown in Figure 2a. If the adiabatic and frictionless processes dominate, the PV anomaly advects conservatively on the isentropic surface [*Hoskins et al.*, 1985]. Because the 320-K Θ surface is approximately located between 300 and 400 hPa for this case, the mismatch between the 320-K IPV contours and 2-PVU surface pressure in Figure 2b suggests the horizontal stretch of the stratospheric intrusion tongue. The discontinuity of the colors denoting the pressure of the 2-PVU surface suggests the degree of the isolation experienced by the STT. By using the 320-K IPV and 2-PVU surface contours, we present a virtual 3-dimensional picture of the stratospheric intrusion and its variation, especially in the later ozone flux analysis. At 1200, in the cutoff cyclone region, the 2-PVU surface pressure was mostly above 450 hPa (~6.2 km) and its contours were consistent with the PV contours. This means that the depressed stratospheric air was not isolated in the troposphere and most of the intrusion was still shallow, although a small amount of the intrusion reached below 500 hPa at the west and south edge of the cutoff low. The horizontal structure of Ozone Monitoring Instrument (OMI) [*Levelt et al.*, 2006] total ozone, in Figure 2c, is consistent with the IPV anomaly distributions with maximum values of >500 DU at both the main and the cutoff cyclones.

[12] Figure 3 shows the pressure-altitude cross-section for (a) Θ and wind speed, and (b) RH, PV, and both the 2-PVU dynamic (black line) and thermal tropopause (white line) at 86.65°W longitude at 1200 27 April. The *WMO* [1986] based thermal tropopause is calculated by using the lapse rate interpolation method presented by *Reichler et al.* [2003] with uncertainties of approximately 30–40 hPa in the extratropics. The thermal tropopause is approximately 1 km higher than the dynamic tropopause at the north side of the intrusion tongue (>37°N) [*Bethan et al.*, 1996] associated with the cyclonic system, and significantly higher than the dynamic tropopause at the south side of the intrusion tongue in association with the small horizontal scale of the PV anomaly [*Wirth*, 2000]. The PV structures show the distinctive tropopause folding between 35°N and 40°N associated with the cutoff cyclone. Although the intrusion's tongue appears to extend equatorward, it also moved eastward. The jet stream is classically located at the south side above the STT tongue near the tropopause. Large gradients exist in wind speed within the tongue. The RH curtain plot shows moist air

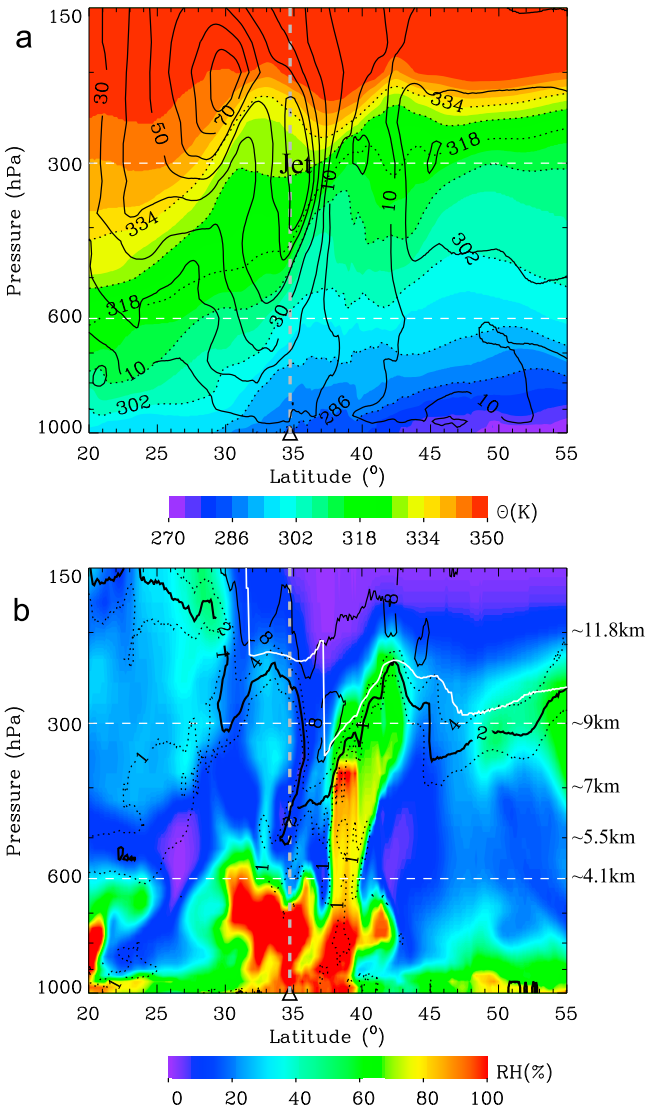

Figure 3. Pressure-altitude cross-section of (a) Θ (color contours) and wind speed (solid black lines); (b) PV (black lines), RH (color contours), and tropopause pressure, at 86.65°W longitude at 1200 UTC 27 April 2010 derived from the NAM model. The PV contour levels include 1, 2, 4, and 8 PVU. The heavy solid black line represents the 2-PVU based dynamic tropopause and the sold white line denotes the WMO thermal tropopause. The latitude of the UAHuntsville lidar station is marked by the black triangle at the bottom.

associated with the surface frontal system beneath the intrusion. Two-way motions, both STT and troposphere-to-stratosphere transport (TST), often occur concurrently. The convective updrafts, which are represented by the high RH column at ~38°N north of the STT tongue in Figure 3b, can potentially transport tropospheric air across tropopause [*Homeyer et al.*, 2011; *Pan et al.*, 2009]. However, no effort is made to quantify the TST in this study. Relative to the cutoff cyclone, the northern intrusion associated with the main cyclone was shallower and has lower wind speeds.

3.2. Measurements

[13] Figure 4 shows the ozone lidar observations, the Θ structures derived from the collocated MPR, and the NAM-derived PV. For correct identification of air-parcel sources, three tropopause heights are presented in Figure 4a: the NAM-derived dynamic tropopause (2-PVU surface, thick black contour), the NAM-derived thermal tropopause (red dashed line), and the MPR-derived thermal tropopause (black crosses). Because the MPR measures temperature only up to 10 km, we made a modification on the WMO definition to calculate the MPR thermal tropopause. If the threshold of 2 $K \cdot km^{-1}$ was detected, the lapse rate of the upper layer was checked up to only 10 km. This adjustment allows tropopause detection between 8 and 10 km albeit with greater uncertainty. The MPR-derived tropopause with 1-min temporal resolution was displayed every 10 min for a better visual result. The ozone profile measured by an ozonesonde launched at 1900 is marked by a black triangle in Figure 4a. The complete plot of ozone, RH, temperature, and tropopause height appears in Figure 5. From the ozonesonde measurement, the WMO-based thermal tropopause is at 6.5 km, 500 m higher than the ozone tropopause, at 6.0 km, derived with either *Bethan et al.*'s [1996] criteria or *Pan et al.*'s [2004] definition.

[14] The STT event with a maximum ozone value of 150-ppbv at 6.5 km was detected by the ozone lidar at ~1600 27 April after a light rain in the early morning (0900–1000). From the PV cross section in Figure 3b, this 1.5-km thick high ozone layer at 6.5 km is the front part of the PV anomaly. Both the 2-PVU surface and the ozone lidar profiles suggest a short-term double tropopause [*Randel et al.*, 2007] at ~6 and ~11 km associated with the PV anomaly. The high ozone mixing ratio and near zero RH above 6 km, shown by the ozonesonde measurement, suggest that the tropopause depressed to ~6 km and the major body of the PV anomaly tongue (shown in Figure 3b) had arrived above Huntsville by 1900. At ~2130, the peak ozone below 10 km seen in the lidar data (Figure 3a), 320 ppbv, occurring at 8 km instead of 9.6 km for the ozonesonde profile suggests the major body of the PV anomaly started to exit the atmosphere above Huntsville. At this tropopause depression phase on 27 April, the PV distribution agrees well with the ozone structures. The dynamic tropopause (2-PVU surface) is approximately consistent with the 100-ppbv ozone surface shown by the lidar and ozonesonde. Although the thermal tropopause generally can represent the center of the transition layer between the stratosphere and troposphere [*Pan et al.*, 2004] on large time and space scales, the NAM-derived thermal tropopause does not show a depressed tropopause to ~6 km despite the same temporal and vertical resolution as the NAM-derived dynamic tropopause, possibly due to the small scale of the horizontal features [*Wirth*, 2000] of the tropopause folding associated with the cutoff cyclone. Moreover, this discrepancy can be caused by the tropopause definitions themselves because the dynamic tropopause captures the changes in both the dynamics and the thermal stratification, while the thermal tropopause captures only the later [*Birner et al.*, 2002; *Wirth*, 2001]. The ozonesonde temperature profile is able to capture the low tropopause indicating that the vertical resolution also affects tropopause identification. After the tropopause depression phase (later than 0000 28 April), the NAM thermal tropopause

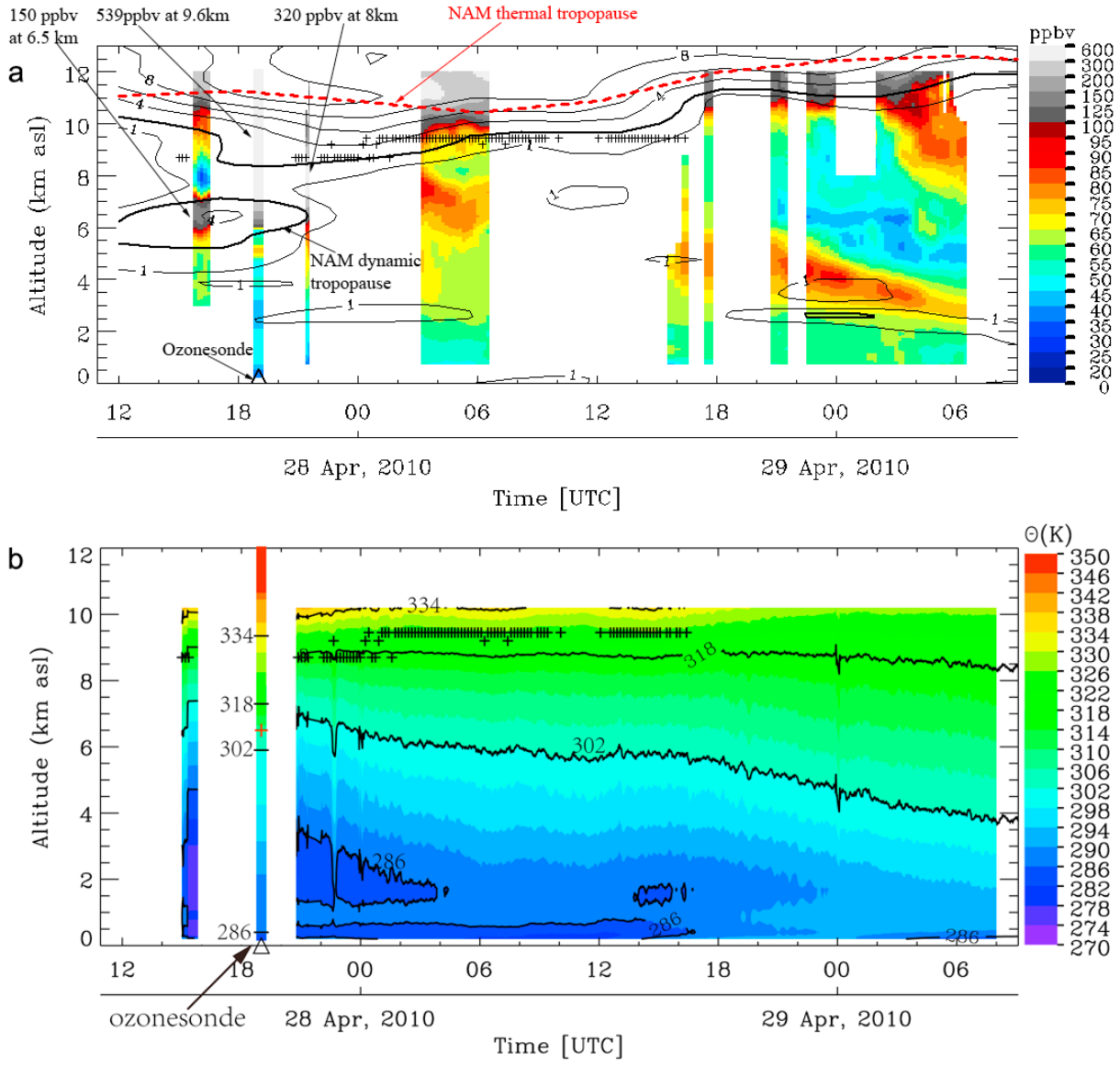

Figure 4. Local measurements of the 27–29 April 2010 STT event in Huntsville. (a) Ozone lidar and ozonesonde (marked by the black triangle at the bottom) measurements. PV contours with 1, 2, 4, 6, 8, and 10-PVU levels (solid black lines), calculated using the 6-h NAM analysis products, are also shown. The thick solid black line delineates the dynamic tropopause (2-PVU surface) and the dashed red line represents the NAM-derived thermal tropopause heights. (b) Θ structures derived from the MPR and ozonesonde. The black and red crosses denote the thermal tropopause heights calculated with the MPR data and ozonesonde, respectively. In some time ranges, no MPR-derived tropopause is present, meaning that the tropopause could exceed the highest detection range of the MPR, 10 km.

is approximately 1–1.5 km higher than the dynamic tropopause and the MPR-derived tropopause. The 1.5-km discrepancy between the MPR-derived thermal tropopause and the NAM-derived thermal tropopause may result from differences in the vertical resolution [*Birner et al.*, 2002] and uncertainty in MPR measurements.

[15] Intermittent precipitation and low level clouds (2–3 km) were found during the daytime on 27 April associated with the surface frontal system located south of Indiana and Ohio, corresponding to the cutoff cyclone. We notice that the lidar observations of 60–65 ppbv ozone between 3 and 4 km at 1600 is about 10–15 ppbv higher than the sonde-observed ozone (~50 ppbv) at 1900 on the same day. This 10–15 ppbv difference has exceeded the measurement uncertainty and, therefore, should be considered to be real because of the quick dilution and convection. The whole tropospheric ozone record shows enormous variability between 1600 and ~2130 associated with the physical mixing processes [*Newell et al.*, 1999; *Oltmans et al.*, 1996].

[16] Ozone lidar measurements made after nighttime precipitation show a descending belt of high ozone with a thickness between 1 and 2 km, which was extruded from the stratosphere and was diluted through turbulence [*Bertin et al.*, 2001]. This ozone rich layer between 70 and 85 ppbv at

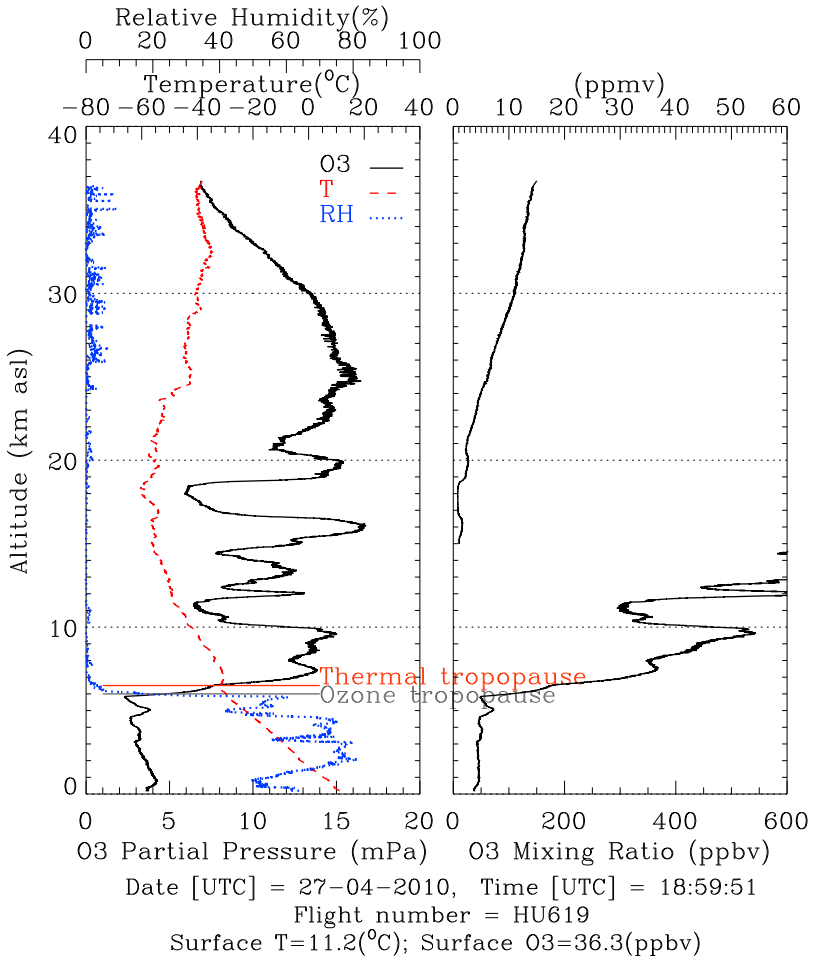

Figure 5. Ozone, temperature (T), and RH profiles measured by ozonesonde at 1900 UTC 27 April 2010 in Huntsville. The thermal tropopause calculated with the *WMO* [1986] definition is 6.5 km, 500 m higher than the ozone tropopause, 6.0 km, derived using either *Pan et al.*'s [2004] definition or *Bethan et al.*'s [1996] criteria.

~7.5 km at 0300 28 April has a Θ between 302 and 310 K (as determined from the coincident MPR measurements), close to the average Θ where STT is most intense for springtime, ~305 K [*Sprenger and Wernli*, 2003]. The Θ of the thermal tropopause (red cross in Figure 4b) derived from the ozonesonde at 1900 the previous afternoon is 297 K. This Θ difference implies that the peak cross-tropopause activity took place slightly (~1 km) above the tropopause found by the ozonesonde [*Hoor et al.*, 2002; *Pan et al.*, 2004, 2006]. The ozone rich layer finally descended to the ~298-K Θ surface at ~2.5 km at 0615 29 April with a rate of ~5 km/day. The STT ozone descended faster than the isentropic surface because of the fact that the exchange processes are not purely dry adiabatic.

[17] Another important variation in Figure 4 is that the upper tropospheric ozone that existed above the STT layer before 1800 on 28 April decreased from ~60–70 to ~40–50 ppbv the second day following intermittent precipitation between 1800 and 2200 on 28 April. To understand this change, we employ HYSPLIT ensemble backward trajectories (R. R. Draxler and G. D. Rolph, HYSPLIT (HYbrid Single-Particle Lagrangian Integrated Trajectory) Model access via NOAA ARL READY Web site (http://ready.arl.noaa.gov/HYSPLIT.php), 2012; G. D. Rolph, Real-time Environmental Applications and Display sYstem (READY) Web site (http://ready.arl.noaa.gov), 2012) to identify the air source regions. As shown by the 72-h backward trajectories ending at 0000 on 29 April 2010 in Figure 6, the 3-km layer originated from the path of the cutoff cyclone and, therefore, had higher ozone, as expected, likely due to the STT. The 6-km air, however, was mostly advected from the mid and low troposphere above Pacific Ocean where the ozone concentration is typically low. The low ozone air after the stratospheric intrusion, even lower than measured before the intrusion, is a common pattern that was frequently observed [e.g., *Roelofs et al.*, 2003] in association with the propagation of the baroclinic waves. STTs associated with tropopause folds usually occur on the western side of the upper-air trough where the northerly or northwesterly winds transport the high-ozone air mass downwind. After the passage of the trough, the westerly winds start to dominate and will advect the air mass, which usually does not contain much stratospheric component or anthropogenic pollution. Therefore, the ozone variation due to STT can be quite complex. The ~80-ppbv layer between 8 and 10 km at 0300 on 29 April likely formed the secondary tongue of the stratospheric air

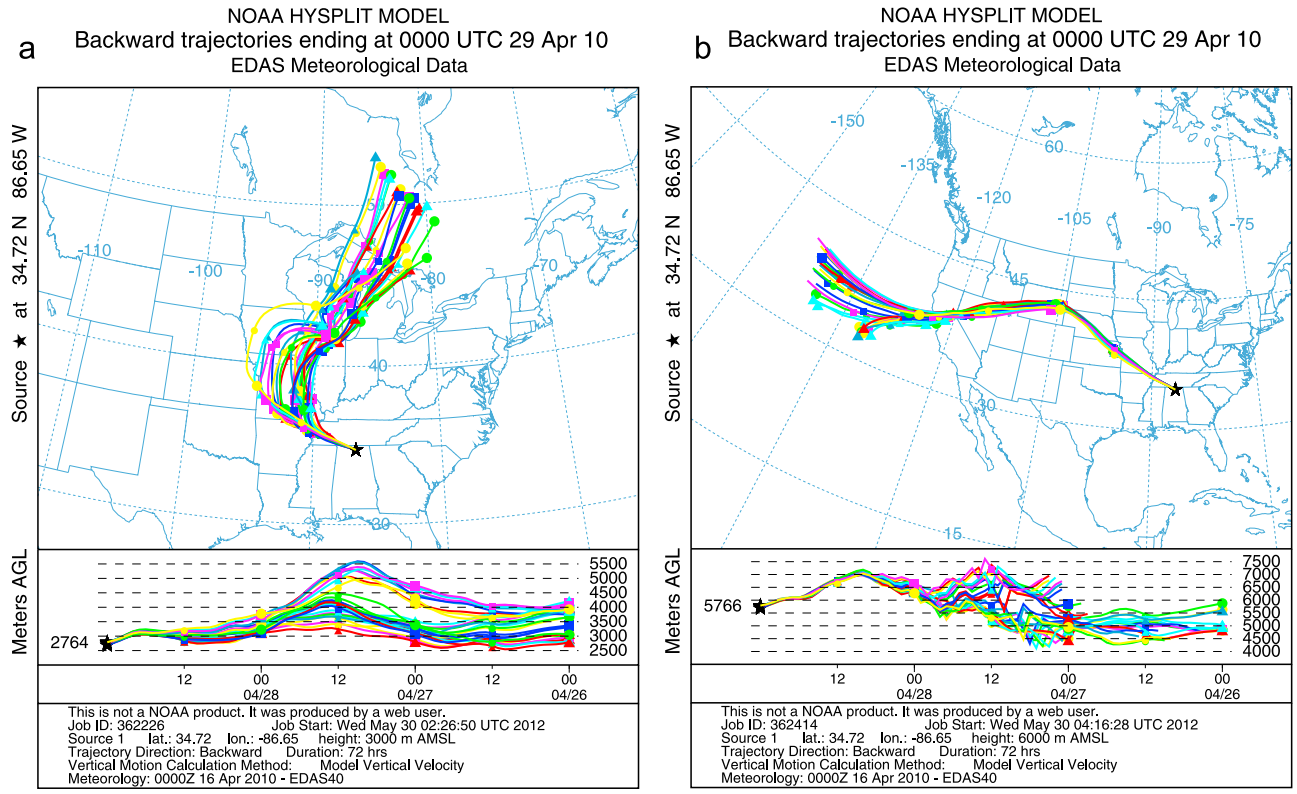

Figure 6. The 72-h HYSPLIT ensemble backward trajectories in Huntsville ending at 0000 29 April 2010 for the layers at (a) 3 km and (b) 6 km asl by using the Eta Data Assimilation System (EDAS) 40-km data from NCEP.

[*Eisele et al.*, 1999]; however, its intrusion is rather shallow without the support of the wind jet.

3.3. Ozone/PV Ratio

[18] The ratio of ozone to PV is an important parameter for modelers to estimate the global STE flux and budget by using PV as an ozone tracer. The ozone/PV ratios in the upper troposphere and lower stratosphere reported by previous investigators differ significantly from 30 to 73 ppbv/PVU with season and location [*Ancellet et al.*, 1994; *Beekmann et al.*, 1994; *Browell et al.*, 1987; *Gouget et al.*, 2000; *Rao et al.*, 2003; *Roelofs and Lelieveld*, 1997]. The ozone/PV ratios reach a maximum in springtime and minimum in winter according to *Beekmann et al.* [1994] primarily associated with the large-scale stratospheric circulation [*Holton et al.*, 1995]. We use both the lidar and ozonesonde measurements to estimate the ozone/PV ratios. The 10-min lidar ozone profiles (in Figure 4a) coinciding with the NAM times are extracted for the calculation. The closest time of NAM reanalysis product to the sounding time (1900) is 1800. This one-hour difference should not be ignored for a quickly moving system. By comparing the moving trajectory of high PV air mass at 1200 and 1800, we believe the ozonesonde measured air approximately at 87.20°W, 35.15°N, which is 0.55° west and 0.43° north of Huntsville, although we understand that the ozonesonde drifted horizontally away from Huntsville during ascent. The ozone is interpolated on the NAM pressure levels. Based on the PV contours and ozone curtain in Figure 4a, the air with PV between 1 and 6 PVU

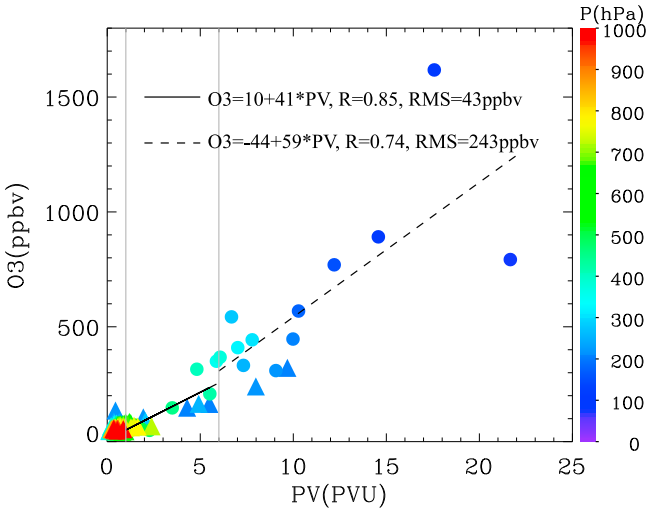

Figure 7. Correlation of NAM-derived PV and measured ozone above Huntsville for 27–29 April 2010, including both the lidar (triangles) and ozonesonde (solid circles) observations. The colors represent pressure. The solid line denotes the correlation derived with PV between 1 and 6 PVU where the mixing of the stratosphere and troposphere occurs. The dashed line represents the correlation calculated using PV greater than 6 PVU where the stratospheric ozone dominates.

can be considered as a mixing layer of the troposphere and stratosphere, with PV greater than 6 PVU indicating stratospheric air dominates.

[19] Figure 7 shows the linear fits for the NAM-derived PV and locally measured ozone above Huntsville, including both the lidar and ozonesonde observations. In the mixing layer of the troposphere and stratosphere, the ozone/PV ratio is equal to 41 ppbv/PVU with a RMS error of 43 ppbv translating to an estimated uncertainty of 33% for an average PV of ~3 PVU. This ozone/PV ratio is close to the climatological average that *Beekmann et al.* [1994] reported for the 225-hPa level (around the lower stratosphere) and springtime for the Observatoire de Haute Provence (OHP) (44°N). However, this ratio is significantly higher than what *Pittman et al.* [2009] reported for the Stratosphere-Troposphere Analyses of Regional Transport 2008 (START08) experiment [*Pan et al.*, 2010] for April–June over North America, ~31 ppbv/PVU. This discrepancy may be the result of an insufficient number of data points in this study. Moreover, the discrepancy could be attributed to the latitude dependence of ozone/PV ratios [*Rao et al.*, 2003] and the error in the latitude/longitude registration for the ozonesonde. The ozone/PV ratio in the stratosphere is ~59 ppbv/PVU. We do not extend the discussion into the stratosphere due to insufficient data for this case.

3.4. STT Flux

[20] Previous estimates of ozone flux originating with STTs vary widely from 0.014 Tg (1.8×10^{32} molecules) to 0.08 Tg (10.4×10^{32} molecules) per day [*Beekmann et al.*, 1997], with the variation attributable to the varying tropopause folding strength, annual variability, and the uncertainty in the calculation method. Figure 8 shows the evolution of the 320-K IPV and the 2-PVU based tropopause pressure from 1800 27 April to 0000 29 April with a 6-h interval (1200 27 April already shown in Figure 2). During this 36-h period, the cutoff low moved along the edge of the main trough and finally merged with it. At 1800 27 April (Figure 8a), the depressed stratospheric air associated with the cutoff cyclone was above 500 hPa (~5.5 km), close to the high PV center at the 320-K Θ surface. At 0600 28 April (Figure 8c), when the elongated high PV region moved to the east side of the main trough from the south side, a large amount of STT air that intruded below 600 hPa was positioned above southern Georgia and far away from the high PV center. This air appears to have been mostly isolated in the troposphere based on the large gradients of the 2-PVU surface pressure (represented by color discontinuity). Six hours later, most of the isolated stratospheric air had been transported over the Atlantic and a portion of it had intruded into the lower troposphere. Figures 8c–8e strongly suggest that the detached stratospheric air, which was located in the low altitude level and represented by red color, had been irreversibly mixed down into the troposphere. We notice that the tropopause pressures for most of the high PV (>2 PVU) region were always between 350 and 400 hPa (green color). This means that air above ~350 hPa (~8 km) most likely remained in the stratosphere regardless of whether the intrusion was isolated.

[21] To estimate the ozone flux associated with this STT event, we assume the linear relationship between PV and ozone derived in the previous section, and furthermore that all of the stratospheric air (>2 PVU) below 375 hPa (~7.5 km) had irreversibly mixed into the troposphere for this relatively small-scale system. This assumption is consistent with the lidar observations which show that the ozone originating from the stratosphere started to descend from ~7.5 km (0300 28 April in Figure 4a). Moreover, this irreversible mixing is strongly suggested by the distinct separation of the thermal and dynamic tropopause [*Pan et al.*, 2007].

[22] Focusing on only the cutoff cyclone system, the calculation area is limited to the square formed by the coordinates (102°W, 80°W) and (33°N, 42.5°N) in Figure 2b. Thus, for 1200 27 April, the estimated stratospheric air, which potentially can be irreversibly transported into the troposphere, was 3.7×10^{14} kg which includes 0.09 Tg (1.13×10^{33} molecules) of ozone. One can calculate the average volume mixing ratio for this STT air reservoir as 148 ppbv (or 3.07 PVU). In this manner, Table 1 gives the potential irreversible STT ozone budget corresponding to the cutoff cyclone for different times. The appropriate spatial areas for this calculation are designated by the white squares in Figure 8. The stratospheric ozone depressed under 375 hPa slightly increases from 1200 27 April to 0000 28 April, consistent with the deeper intrusion shown in Figure 8. However, the stratospheric ozone under 375 hPa significantly decreased from 0.106 Tg at 0000 28 April to 0.073 Tg six hours later, then to 0.035 Tg twelve hours later. The ozone mass differences for each 6-h period were associated with the irreversible mixed stratospheric ozone that had lost the characteristics of stratosphere air (e.g., PV > 2 PVU). Due to its dilution, the average ozone mixing ratio of the air originating from the stratosphere with PV greater than 2 PVU decreased from 150 ppbv at 0000 28 April to 112 ppbv at 1800 28 April. This result is consistent with the lidar observations and NAM-derived PV structures in Huntsville that show the air with ozone less than 100 ppbv generally had PV less than 2 PVU. These results suggest that, if the stratospheric air is irreversibly transported across the tropopause, it will quickly lose its stratospheric characteristics [*Stohl et al.*, 2000], such as high PV and high ozone, due to the quick mixing with surrounding tropospheric air so that it is difficult to track the STT air with these tracers more than a few days.

[23] Table 1 indicates that the intense irreversible mixing started to occur between 0000 and 0600 28 April, consistent with the ozone lidar observations in Figure 4a. The stratospheric intrusion tongue at 0600 28 April (Figure 8c) was almost completely detached, while the intrusion tongue at 1200 28 April (Figure 8b) had lower possibility of being completely mixed down. The ozone in the stratospheric intrusion tongue above two times can be seen as the lower and upper bound, respectively. Thereby, the contribution of the STT to the troposphere is approximately between 0.106 Tg and 0.073 Tg during a two-day period. We consider the lifetime of the cutoff low as the STT timescale. In this study, we did not consider TST because the STT dominates the process and the revolution of the PV anomalies does not show that the detached intrusion tongue returned to the stratosphere as *Vaughan et al.* [1994] saw. The upper bound of the STT budget estimate from this study is close to what *Lamarque and Hess* [1994] reported (0.11 Tg) for a similar cutoff low system, which had a lifetime about four days, during later wintertime. However, *Lamarque and Hess*

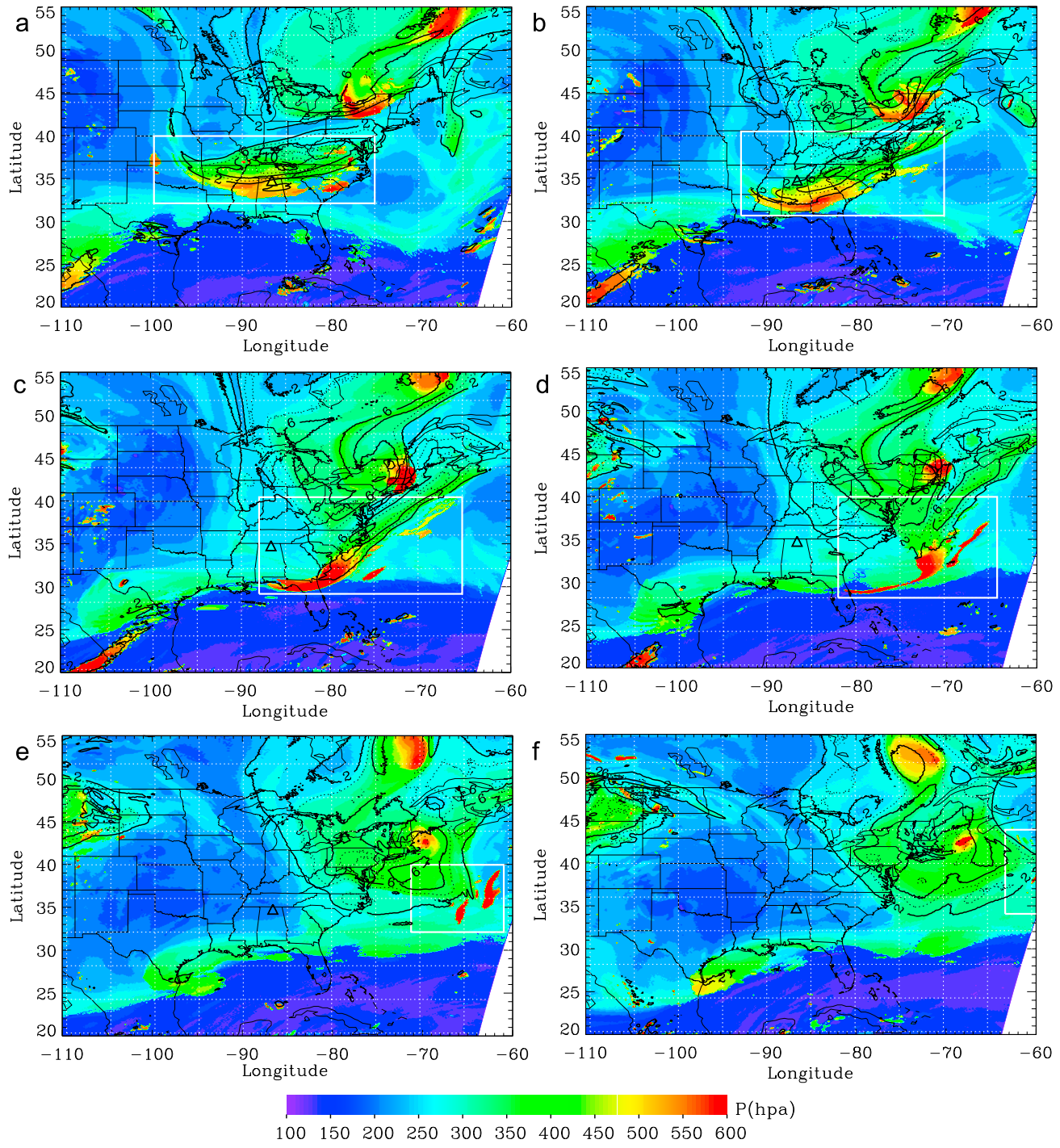

Figure 8. NAM derived 320-K IPV (black dotted and solid interweaved contours) and the 2-PVU tropopause pressure (color contours) for (a) 1800 27 April, (b) 0000 28 April, (c) 0600 28 April, (d) 1200 28 April, (e) 1800 28 April, and (e) 0000 29 April. The white squares designate the area for the STT budget calculation. The mismatch of the contours of 320-K IPV and the lowest 2-PV pressure suggest the extension of the stratospheric intrusion tongue in the troposphere.

[1994] calculated the two-way transport using a meso-scale model, including both STT and TST. The budget from this study is about twice what *Langford et al.* [1996] reported for an October cutoff low, ~0.04 Tg, over a larger geographical area and higher PV. *Cooper et al.* [2004] reported a 0.5 Tg ozone contribution during 7.5 days (60% of the irreversible mixing happens within 2 days) from a springtime STT event associated with a larger cyclonic system, and by using a higher ozone/PV ratio and a different approach compared with this study. Not surprisingly, as the sensitivity tests have shown, the major uncertainty for this calculation arises from assumptions about the location of the pressure level at which

Table 1. Potential Irreversible STT Ozone Budget

Time	Figure for Analysis	Potential Irrevsersible STT Ozone (10^{33} Molecules)	Potential Irrevsersible STT Ozone (Tg)	Average Ozone/PV Ratio in the Reservoir (ppbv/PVU)	Average Ozone Mixing Ratio in the Reservoir[a] (ppbv)
1200 27 April	Figure 2b	1.13	0.090	3.07	148
1800 27 April	Figure 8a	1.21	0.096	3.02	145
0000 28 April	Figure 8b	1.33	0.106	3.10	150
0600 28 April	Figure 8c	0.92	0.073	2.99	142
1200 28 April	Figure 8d	0.44	0.035	2.51	115
1800 28 April	Figure 8e	0.16	0.013	2.47	112
0000 29 April	Figure 8f	0.01	0.001	2.24	99

[a]The correlation relationship between ozone and PV is $O_3 = 10 + 41 \times$ PV (ppbv) which is derived with PV between 1 and 6 PVU and shown in Figure 7.

irreversible mixing occurred. If this level is assumed to be 350 hPa, the STT ozone contribution will be 50% higher. The second uncertainty, estimated to be ~33%, comes from the linear relationship between IPV and ozone. The combined uncertainty for the above two sources is approximately 59%. The final uncertainty for the flux calculation could be even higher due to the uncertainty in the time period estimate.

3.5. Impact on Ozone Vertical Profile and Variability

[24] As shown by Figure 4, the ozone measured by the lidar and ozonesonde within the first 12 h after the stratospheric intrusion exhibits considerable variability in the mid and upper troposphere. Most of the lower tropospheric ozone variation is associated with intense advection and convection processes. The ozone variation associated with STT is rather complicated. We see that the STT occurred over Huntsville at 1200 27 April as shown in Figure 3. To help understand the ozone variability, we calculate average ozone values using the 10-min lidar profiles and their 1-σ standard deviation for the two observational periods, from 0300 to 0645 28 April (~15–19 h after the intrusion) and from 2230 28 April to 0630 29 April (~35–43 h after the intrusion). There was no low-cloud interference for these two periods. The average ozone profiles for these two periods plotted in Figure 9 clearly show the STT air transported between ~7 to ~3.5 km and an ~15-ppbv ozone decrease in the upper troposphere due to westerly advection. For the 15–19 h lidar measurements, the 10-min ozone profiles exhibit slightly higher variability (~6%) in the STT ozone layer, 5.5–8 km, and the variability in the lower layer, where the STT effect is negligible, is less than 4%. However, for the 35–43 h lidar data, the variability can be as large as 22% (near 4.5 km) mostly due to the westerly low ozone flow. This result suggests that the variability in the upper atmosphere is rather small after the stratospheric intrusion tongue has dissipated and that much larger variability could be seen later at the transition of the prevailing wind flow.

3.6. Impact on the Surface

[25] To investigate the STE impact on surface ozone levels, we analyzed the EPA hourly surface ozone monitoring data from the Air Quality System. The 1-h maximum surface ozone at most EPA stations, including high elevation stations and the stations that have minimum anthropogenic emissions in Alabama and Georgia, was ~40, ~50, and 60 ppbv on 27, 28, and 29 April respectively. This gradual ozone enhancement is mostly related to the development of the high-pressure system. There is no abnormal surface ozone jump or geographic distribution pattern which can be attributed to this STT event. Therefore, we believe that this STT event does not have an immediate impact on surface ozone within the PBL. However, exchange processes between the PBL and the free troposphere always exist and can affect surface levels after injecting free tropospheric ozone into the nocturnal PBL [*Morris et al.*, 2010]. In Figure 4a, the PBL ozone exhibits primarily a diurnal variation after 0300 28 April except for a slight enhancement (~5 ppbv) observed between 0100 and 0400 on 29 April due to the downward flux following the collapse of the convective boundary layer top.

4. Conclusions

[26] The UAHuntsville ozone lidar and ozonesondes captured a springtime STT event associated with an upper-air cutoff cyclone and tropopause fold. The jet stream with maximum winds of ~60 m/s was classically located at the southern edge above the stratospheric intrusion tongue near the tropopause. The observed tropopause in Huntsville descended to ~6 km in the direct stratospheric intrusion stage and then ascended to ~10 km after ~12 h.

[27] The PV anomalies calculated from the analysis data of NCEP's NAM model [*Janjic*, 2003] with 6-h intervals agree well with the ozone observations in Huntsville. The NAM-derived 2-PVU surface, defined as the dynamic tropopause in this work, generally coincides with the ozone tropopause estimated from the ozonesonde and lidar measurements consistent with previous studies [e.g., *Krebsbach et al.*, 2006]. The NAM-derived thermal tropopause based on the *WMO* [1986] definition fails to reproduce the depressed tropopause possibly due to the "cyclone-anticyclone asymmetry" associated with the small-scale cyclonic system, as described by *Wirth* [2000, 2001].

[28] After the direct intrusion phase, the lidar observed a 2-km thick elevated ozone layer at ~7.5 km with values between 70 and 85 ppbv, resulting from the STT. The Θ (302–310 K) of this ozone rich layer is higher than that at the tropopause, calculated from the earlier ozonesonde profile, suggesting that the intense cross-tropopause activities took place slightly higher than the tropopause [*Hoor et al.*, 2002; *Pan et al.*, 2004, 2006]. This ozone rich layer descended to the 298-K Θ surface (~2.5 km) at a rate of ~5 km/day.

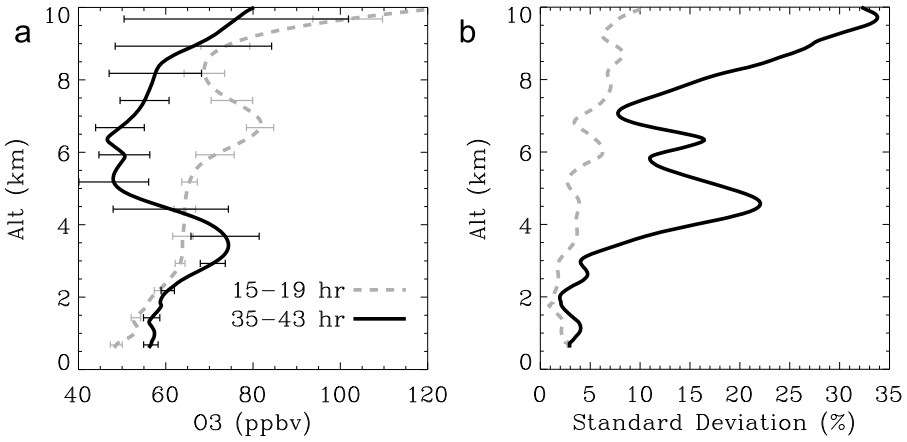

Figure 9. Variability of the ozone lidar measurements in Figure 5. (a) Average ozone of the 10-min lidar profiles and its 1-σ standard deviation. The gray dashed line represents the observation duration from 0300 to 0645 28 April (∼15–19 h after the intrusion) and the black solid line represents the observation duration from 2230 28 April to 0630 29 April (∼35–43 h after the intrusion). The interval of the standard deviation is 750 m which represents the vertical resolution of the lidar measurements. (b) The 1-σ standard deviation of the two periods in unit of percentage.

According to the lidar measurements in Figure 4a and the evolution of PV anomalies in Figure 8, once the stratospheric air is irreversibly transported to the troposphere, it quickly loses its stratospheric characteristics (e.g., PV > 2, high ozone, high Θ) [*Stohl et al.*, 2000] due to the dilution with surrounding air indicating that it is difficult to track the stratospheric air with the tracers and accurately quantify the influence of STT on the troposphere.

[29] We divide the air into two categories: the mixing layer between the stratosphere and troposphere with PV between 1 and 6 PVU; and the stratosphere with PV greater than 6 PVU. By the least squares fits of the NAM-derived PV and measured ozone, the ozone/PV ratio for the mixing layer is ∼41 ppbv/PVU with an estimated error of 33%, which is close to the climatological average that *Beekmann et al.* [1994] reported the for springtime. However, this ratio is significantly higher than what *Pittman et al.* [2009] reported for the START08 experiment [*Pan et al.*, 2010]. This ratio is expected to be more accurate with more comprehensive data in the future.

[30] During this two-day period, the estimated ozone irreversibly transported from the stratospheric into the troposphere is between 0.07 Tg (0.9×10^{33} molecules) and 0.11 Tg (1.3×10^{33} molecules) with an estimated uncertainty of 59%. The uncertainty in the ozone budget could be significantly reduced by supplying simultaneous measurements from multiple stations to a high resolution model.

[31] Tropospheric ozone above Huntsville exhibited enormous variability due to the horizontal and vertical mixing processes. Low ozone and large variability were observed in the mid-troposphere after the stratospheric intrusion due to the westerly advection when the transition from the cyclonic system to anticyclonic system. We did not find any significant impact from this event on surface ozone when looking at the EPA hourly surface data. This conclusion is consistent with the lidar ozone observations showing that the high ozone layer originating from the stratosphere did not extend to the daytime boundary layer. Although the direct stratospheric intrusion lasts for a period extending from several hours to a few days [*Bithell et al.*, 2000; *Cooper et al.*, 2004], its indirect impact on the lower troposphere could be much longer [*Liang et al.*, 2009].

[32] **Acknowledgments.** The authors would like to thank Tom McGee of NASA/GSFC, Stuart McDermid and Thierry Leblanc of NASA/JPL for extensive discussions about lidar instrumentation, Wesley Cantrell of UAHuntsville for providing the ozonesonde data, and the NASA/GSFC OMI working group for providing the OMI column ozone data. This work was supported by NASA's Science Mission Directorate and NOAA's National Environmental Satellite, Data, and Information Service (NESDIS). The UAHuntsville RAPCD ozone lidar is affiliated with the Network for Detection of Atmospheric Composition Change (NDACC), and its data are publicly available at http://www.ndacc.org and http://nsstc.uah.edu/atmchem.

References

Ancellet, G., J. Pelon, M. Beekmann, A. Papayannis, and G. Megie (1991), Ground-based lidar studies of ozone exchanges between the stratosphere and the troposphere, *J. Geophys. Res.*, *96*, 22,401–22,421, doi:10.1029/91JD02385.

Ancellet, G., M. Beekmann, and A. Papayannis (1994), Impact of a cut-off low development on downward transport of ozone in the troposphere, *J. Geophys. Res.*, *99*(D2), 3451–3468, doi:10.1029/93JD02551.

Beekmann, M., G. Ancellet, and G. Mégie (1994), Climatology of tropospheric ozone in the southern Europe and its relation to potential vorticity, *J. Geophys. Res.*, *99*, 12,841–12,853, doi:10.1029/94JD00228.

Beekmann, M., et al. (1997), Regional and global tropopause fold occurrence and related ozone flux across the tropopause, *J. Atmos. Chem.*, *28*, 29–44, doi:10.1023/A:1005897314623.

Bertin, F., B. Campistron, J. L. Caccia, and R. Wilson (2001), Mixing processes in a tropopause folding observed by a network of ST radar and lidar, *Ann. Geophys.*, *19*, 953–963, doi:10.5194/angeo-19-953-2001.

Bethan, S., G. Vaughan, and S. J. Reid (1996), A comparison of ozone and thermal tropopause heights and the impact of tropopause definition on quantifying the ozone content of the troposphere, *Q. J. R. Meteorol. Soc.*, *122*, 929–944, doi:10.1002/qj.49712253207.

Birner, T., A. Dörnbrack, and U. Schumann (2002), How sharp is the tropopause at midlatitudes?, *Geophys. Res. Lett.*, *29*(14), 1700, doi:10.1029/2002GL015142.

Bithell, M., G. Vaughan, and L. J. Gray (2000), Persistence of stratospheric ozone layers in the troposphere, *Atmos. Environ.*, *34*, 2563–2570, doi:10.1016/S1352-2310(99)00497-5.

Browell, E. V., E. F. Danielsen, S. Ismail, G. L. Gregory, and S. M. Beck (1987), Tropopause fold structure determinded from airborne lidar and in situ measurements, *J. Geophys. Res.*, *92*, 2112–2120, doi:10.1029/JD092iD02p02112.

Browell, E. V., et al. (1996), Ozone and aerosol distributions and air mass characteristics over the South Atlantic Basin during the burning season, *J. Geophys. Res.*, *101*(D19), 24,043–24,068, doi:10.1029/95JD02536.

Cooper, O., et al. (2004), On the life cycle of a stratospheric intrusion and its dispersion into polluted warm conveyor belts, *J. Geophys. Res.*, *109*, D23S09, doi:10.1029/2003JD004006.

Danielsen, E. F. (1968), Stratosphere-troposphere exchange based on radioactivity, ozone and potential vorticity, *J. Atmos. Sci.*, *25*, 502–518, doi:10.1175/1520-0469(1968)025<0502:STEBOR>2.0.CO;2.

Dethof, A., A. O'Neill, and J. Slingo (2000), Quantification of the isentropic mass transport across the dynamical tropopause, *J. Geophys. Res.*, *105*(D10), 12,279–12,293, doi:10.1029/2000JD900127.

Eisele, H., H. E. Scheel, R. Sladkovic, and T. Trickl (1999), High-resolution lidar measurements of stratosphere-troposphere exchange, *J. Atmos. Sci.*, *56*, 319–330, doi:10.1175/1520-0469(1999)056<0319:HRLMOS>2.0.CO;2.

Fusco, A., and J. A. Logan (2003), Analysis of 1970–1995 trends in tropospheric ozone at Northern Hemisphere midlatitudes with the GEOS-CHEM model, *J. Geophys. Res.*, *108*(D15), 4449, doi:10.1029/2002JD002742.

Gouget, H., G. Vaughan, A. Marenco, and H. G. J. Smit (2000), Decay of a cut-off low and contribution to the stratosphere-troposphere exchange, *Q. J. R. Meteorol. Soc.*, *126*, 1117–1141.

Güldner, J., and D. Spänkuch (2001), Remote sensing of the thermodynamic state of the atmospheric boundary layer by ground-based microwave radiometry, *J. Atmos. Oceanic Technol.*, *18*, 925–933, doi:10.1175/1520-0426(2001)018<0925:RSOTTS>2.0.CO;2.

Hoerling, M. P., T. K. Schaack, and A. J. Lenzen (1991), Global objective tropopause analysis, *Mon. Weather Rev.*, *119*, 1816–1831, doi:10.1175/1520-0493(1991)119<1816:GOTA>2.0.CO;2.

Hoinka, K. P. (1998), Statistics of the global tropopause pressure, *Mon. Weather Rev.*, *126*, 3303–3325, doi:10.1175/1520-0493(1998)126<3303:SOTGTP>2.0.CO;2.

Holton, J. R., P. H. Haynes, M. E. McIntyre, A. R. Douglass, R. B. Rood, and L. Pfister (1995), Stratosphere-troposphere exchange, *Rev. Geophys.*, *33*, 403–440, doi:10.1029/95RG02097.

Homeyer, C., K. Bowman, L. Pan, E. Atlas, R. Gao, and T. Campos (2011), Dynamical and chemical characteristics of tropospheric intrusions observed during START08, *J. Geophys. Res.*, *116*, D06111, doi:10.1029/2010JD015098.

Hoor, P., H. Fischer, L. Lange, J. Lelieveld, and D. Brunner (2002), Seasonal variations of a mixing layer in the lowermost stratosphere as identified by the CO-O_3 correlation from in situ measurements, *J. Geophys. Res.*, *107*(D5), 4044, doi:10.1029/2000JD000289.

Hoskins, B. J., M. E. McIntyre, and A. W. Robertson (1985), On the use and significance of isentropic potential-vorticity maps, *Q. J. R. Meteorol. Soc.*, *111*, 877–946, doi:10.1256/smsqj.47001.

Hsu, J., M. J. Prather, and O. Wild (2005), Diagnosing the stratosphere-to-troposphere flux of ozone in a chemistry transport model, *J. Geophys. Res.*, *110*, D19305, doi:10.1029/2005JD006045.

James, P., A. Stohl, C. Forster, S. Eckhardt, P. Seibert, and A. Frank (2003), A 15-year climatology of stratosphere–troposphere exchange with a Lagrangian particle dispersion model. 2. Mean climate and seasonal variability, *J. Geophys. Res.*, *108*(D12), 8522, doi:10.1029/2002JD002639.

Janjic, Z. I. (2003), A nonhydrostatic model based on a new approach, *Meteorol. Atmos. Phys.*, *82*, 271–285, doi:10.1007/s00703-001-0587-6.

Johnson, B. J., S. J. Oltmans, H. Vömel, H. G. J. Smit, T. Deshler, and C. Kröger (2002), Electrochemical concentration cell (ECC) ozonesonde pump efficiency measurements and tests on the sensitivity to ozone of buffered and unbuffered ECC sensor cathode solutions, *J. Geophys. Res.*, *107*(D19), 4393, doi:10.1029/2001JD000557.

Johnson, B. J., D. Helmig, and S. Oltmans (2008), Evaluation of ozone measurements from a tethered balloon-sampling platform at South Pole Station in December 2003, *Atmos. Environ.*, *42*, 2780–2787, doi:10.1016/j.atmosenv.2007.03.043.

Karan, H., and K. Knupp (2006), Mobile Integrated Profiler System (MIPS) observations of low-level convergent boundaries during IHOP, *Mon. Weather Rev.*, *134*, 92–112, doi:10.1175/MWR3058.1.

Knupp, K. (2006), Observational analysis of a gust front to bore to solitary wave transition within an evolving nocturnal boundary layer, *J. Atmos. Sci.*, *63*, 2016–2035, doi:10.1175/JAS3731.1.

Knupp, K. R., R. Ware, D. Climini, F. Vandenberghe, J. Vivekanandan, E. Westwater, T. Coleman, and D. Phillips (2009), Ground-based passive microwave profiling during dynamic weather conditions, *J. Atmos. Oceanic Technol.*, *26*, 1057–1073, doi:10.1175/2008JTECHA1150.1.

Komhyr, W. D. (1969), Electrochemical cells for gas analysis, *Ann. Geophys.*, *25*, 203–210.

Komhyr, W. D., R. A. Barnes, G. B. Brothers, J. A. Lanthrop, and D. P. Opperman (1995), Electrochemical concentration cell ozonesonde performance evaluation during STOIC 1989, *J. Geophys. Res.*, *100*, 9231–9244, doi:10.1029/94JD02175.

Krebsbach, M., et al. (2006), Seasonal cycles and variability of O_3 and H_2O in the UT/LMS during SPURT, *Atmos. Chem. Phys.*, *6*, 109–125, doi:10.5194/acp-6-109-2006.

Kuang, S., J. F. Burris, M. J. Newchurch, S. Johnson, and S. Long (2011a), Differential Absorption Lidar to measure subhourly variation of tropospheric ozone profiles, *IEEE Trans. Geosci. Remote Sens.*, *49*, 557–571, doi:10.1109/TGRS.2010.2054834.

Kuang, S., et al. (2011b), Nocturnal ozone enhancement in the lower troposphere observed by lidar, *Atmos. Environ.*, *45*, 6078–6084, doi:10.1016/j.atmosenv.2011.07.038.

Lamarque, J.-F., and P. G. Hess (1994), Cross-tropopause mass exchange and potential vorticity budget in a simulated tropopause folding, *J. Atmos. Sci.*, *51*, 2246–2269, doi:10.1175/1520-0469(1994)051<2246:CTMEAP>2.0.CO;2.

Lamarque, J.-F., A. O. Langford, and M. H. Proffitt (1996), Cross-tropopause mixing of ozone through gravity wave breaking: Observation and modeling, *J. Geophys. Res.*, *101*, 22,969–22,976, doi:10.1029/96JD02442.

Langford, A. O., C. D. Masters, M. H. Proffitt, E.-Y. Hsie, and A. F. Tuck (1996), Ozone measurements in a tropopause fold associated with a cut-off low system, *Geophys. Res. Lett.*, *23*, 2501–2504, doi:10.1029/96GL02227.

Langford, A. O., K. Aikin, C. S. Eubank, and E. J. Williams (2009), Stratospheric contribution to high surface ozone in Colorado during springtime, *Geophys. Res. Lett.*, *36*, L12801, doi:10.1029/2009GL038367.

Lefohn, A., H. Wernli, D. S. Shadwick, S. Limbach, S. Oltmans, and M. Shapiro (2011), The importance of stratospheric-tropospheric transport in affecting surface ozone concentrations in the western and northern tier of the United States, *Atmos. Environ.*, *45*, 4845–4857, doi:10.1016/j.atmosenv.2011.06.014.

Lelieveld, J., and F. J. Dentener (2000), What controls tropospheric ozone?, *J. Geophys. Res.*, *105*, 3531–3551, doi:10.1029/1999JD901011.

Levelt, P. F., G. H. J. van den Oord, M. R. Dobber, A. Mälkki, H. Visser, J. de Vries, P. Stammes, J. O. V. Lundell, and H. Saari (2006), The Ozone Monitoring Instrument, *IEEE Trans. Geosci. Remote Sens.*, *44*, 1093–1101, doi:10.1109/TGRS.2006.872333.

Liang, Q., A. R. Douglass, B. Duncan, R. Stolarski, and J. Witte (2009), The governing processes and timescales of stratosphere-to-troposphere transport and its contribution to ozone in the Arctic troposphere, *Atmos. Chem. Phys.*, *9*, 3011–3025, doi:10.5194/acp-9-3011-2009.

Monks, P. S. (2000), A review of the observations and origins of the spring ozone maximum, *Atmos. Environ.*, *34*, 3545–3561, doi:10.1016/S1352-2310(00)00129-1.

Morris, G. A., B. Ford, B. Rappenglück, A. M. Thompson, A. Mefferd, F. Ngan, and B. Lefer (2010), An evaluation of the interaction of morning residual layer and afternoon mixed layer ozone in Houston using ozonesonde data, *Atmos. Environ.*, *44*, 4024–4034, doi:10.1016/j.atmosenv.2009.06.057.

Newchurch, M. J., M. A. Ayoub, S. Oltmans, B. Johnson, and F. J. Schmidlin (2003), Vertical distribution of ozone at four sites in the United States, *J. Geophys. Res.*, *108*(D1), 4031, doi:10.1029/2002JD002059.

Newell, R. E., V. Thouret, J. Y. N. Cho, P. Stoller, A. Marenco, and H. G. Smit (1999), Ubiquity of quasi-horizontal layers in the troposphere, *Nature*, *398*, 316–319, doi:10.1038/18642.

Nieto, R., et al. (2005), Climatological features of cutoff low systems in the Northern Hemisphere, *J. Clim.*, *18*, 3085–3103, doi:10.1175/JCLI3386.1.

Olsen, M. A., M. R. Schoeberl, and A. R. Douglass (2004), Stratosphere-troposphere exchange of mass and ozone, *J. Geophys. Res.*, *109*, D24114, doi:10.1029/2004JD005186.

Oltmans, S. J., et al. (1996), Summer and spring ozone profiles over the North Atlantic from ozonesonde measurements, *J. Geophys. Res.*, *101*(D22), 29,179–29,200, doi:10.1029/96JD01713.

Pan, L. L., W. J. Randel, B. L. Gary, M. J. Mahoney, and E. J. Hintsa (2004), Definitions and sharpness of the extratropical tropopause: A trace gas perspective, *J. Geophys. Res.*, *109*, D23103, doi:10.1029/2004JD004982.

Pan, L. L., P. Konopka, and E. V. Browell (2006), Observations and model simulations of mixing near the extratropical tropopause, *J. Geophys. Res.*, *111*, D05106, doi:10.1029/2005JD006480.

Pan, L. L., et al. (2007), Chemical behavior of the tropopause observed during the Stratosphere-Troposphere Analyses of Regional Transport experiment, *J. Geophys. Res.*, *112*, D18110, doi:10.1029/2007JD008645.

Pan, L. L., W. J. Randel, J. C. Gille, W. D. Hall, B. Nardi, S. Massie, V. Yudin, R. Khosravi, P. Konopka, and D. Tarasick (2009), Tropospheric

intrusions associated with the secondary tropopause, *J. Geophys. Res.*, *114*, D10302, doi:10.1029/2008JD011374.

Pan, L. L., et al. (2010), The stratosphere-troposphere analyses of regional transport 2008(START08) experiment, *Bull. Am. Meteorol. Soc.*, *91*, 327–342, doi:10.1175/2009BAMS2865.1.

Pittman, J. V., L. L. Pan, J. C. Wei, F. W. Irion, X. Liu, E. S. Maddy, C. D. Barnet, K. Chance, and R.-S. Gao (2009), Evaluation of AIRS, IASI, and OMI ozone profile retrievals in the extratropical tropopause region using in situ aircraft measurements, *J. Geophys. Res.*, *114*, D24109, doi:10.1029/2009JD012493.

Price, J. D., and G. Vaughan (1993), The potential for stratosphere-troposphere exchange in cut-off-systems, *Q. J. R. Meteorol. Soc.*, *119*, 343–365, doi:10.1002/qj.49711951007.

Randel, W. J., D. J. Seidel, and L. L. Pan (2007), Observational characteristics of double tropopauses, *J. Geophys. Res.*, *112*, D07309, doi:10.1029/2006JD007904.

Rao, T. N., S. Kirkwood, J. Arvelius, P. von der Gathen, and R. Kivi (2003), Climatology of UTLS ozone and the ratio of ozone and potential vorticity over northern Europe, *J. Geophys. Res.*, *108*(D22), 4703, doi:10.1029/2003JD003860.

Ravetta, F., G. Ancellet, J. Kowol-Santen, R. Wilson, and D. Dedeljdovic (1999), Ozone, temperature, and wind field measurements in a tropopause fold: comparison with a mesoscale model simulation, *Mon. Weather Rev.*, *127*, 2641–2653, doi:10.1175/1520-0493(1999)127<2641:OTAWFM>2.0.CO;2.

Reichler, T., M. Dameris, and R. Sausen (2003), Determining the tropopause height from gridded data, *Geophys. Res. Lett.*, *30*(20), 2042, doi:10.1029/2003GL018240.

Roelofs, G. J., and J. Lelieveld (1997), Model study of the influence of crosstropopause O^3 transports on tropospheric O^3 levels, *Tellus, Ser. B*, *49*, 38–55.

Roelofs, G. J., et al. (2003), Intercomparison of tropospheric ozone models: Ozone transport in a complex tropopause folding event, *J. Geophys. Res.*, *108*(D12), 8529, doi:10.1029/2003JD003462.

Shapiro, M. A. (1980), Turbulent mixing within tropopause folds as a mechanism for the exchange of the chemical constituents between the stratosphere and troposphere, *J. Atmos. Sci.*, *37*, 994–1004, doi:10.1175/1520-0469(1980)037<0994:TMWTFA>2.0.CO;2.

Smit, H. G. J., et al. (2007), Assessment of the performance of ECC-ozonesondes under quasi-flight conditions in the environmental simulation chamber: Insights from the Juelich Ozone Sonde Intercomparison Experiment (JOSIE), *J. Geophys. Res.*, *112*, D19306, doi:10.1029/2006JD007308.

Solheim, F., J. R. Godwin, E. R. Westwater, Y. Han, S. J. Keihm, K. Marsh, and R. Ware (1998), Radiometric profiling of temperature, water vapor and cloud liquid water using various inversion methods, *Radio Sci.*, *33*(2), 393–404, doi:10.1029/97RS03656.

Sorensen, J. H., and N. W. Nielsen (2001), Intrusion of stratospheric ozone to the free troposphere through tropopause folds - A case study, *Phys. Chem. Earth Part B*, *26*, 801–806.

Sprenger, M., and H. Wernli (2003), A northern hemispheric climatology of cross-tropopause exchange for the ERA15 time period (1979–1993), *J. Geophys. Res.*, *108*(D12), 8521, doi:10.1029/2002JD002636.

Stohl, A., et al. (2000), The influence of stratospheric intrusions on alpine ozone concentrations, *Atmos. Environ.*, *34*, 1323–1354, doi:10.1016/S1352-2310(99)00320-9.

Stohl, A., et al. (2003a), Stratosphere-troposphere exchange: A review and what we learned from STACCATO, *J. Geophys. Res.*, *108*(D12), 8516, doi:10.1029/2002JD002490.

Stohl, A., H. Wernli, P. James, M. Bourqui, C. Forster, M. A. Liniger, P. Seibert, and M. Sprenger (2003b), A new perspective of stratosphere–troposphere exchange, *Bull. Am. Meteorol. Soc.*, *84*, 1565–1573, doi:10.1175/BAMS-84-11-1565.

Thompson, A. M., et al. (2007), Intercontinental Chemical Transport Experiment Ozonesonde Network Study (IONS) 2004: 2. Tropospheric ozone budgets and variability over northeastern North America, *J. Geophys. Res.*, *112*, D12S13, doi:10.1029/2006JD007670.

Vaughan, G., J. D. Price, and A. Howells (1994), Transport into the troposphere in a tropopause fold, *Q. J. R. Meteorol. Soc.*, *120*, 1085–1103, doi:10.1002/qj.49712051814.

Vingarzan, R. (2004), A review of surface ozone background levels and trends, *Atmos. Environ.*, *38*, 3431–3442, doi:10.1016/j.atmosenv.2004.03.030.

Ware, R., R. Carpenter, J. Güldner, J. Liljegren, T. Nehrkorn, F. Solheim, and F. Vandenberghe (2003), A multichannel radiometric profiler of temperature, humidity, and cloud liquid, *Radio Sci.*, *38*(4), 8079, doi:10.1029/2002RS002856.

Wernli, H., and M. Bourqui (2002), A Lagrangian "1-year climatology" of (deep) cross-tropopause exchange in the extratropical Northern Hemisphere, *J. Geophys. Res.*, *107*(D2), 4021, doi:10.1029/2001JD000812.

Wirth, V. (2000), Thermal versus dynamical tropopause in upper-tropospheric balanced flow anomalies, *Q. J. R. Meteorol. Soc.*, *126*, 299–317, doi:10.1002/qj.49712656215.

Wirth, V. (2001), Cyclone-anticyclone asymmetry concerning the height of the thermal and the dynamical tropopause, *J. Atmos. Sci.*, *58*, 26–37, doi:10.1175/1520-0469(2001)058<0026:CAACTH>2.0.CO;2.

World Meteorological Organization (WMO) (1986), Atmospheric ozone 1985, *WMO Global Ozone Res. and Monit. Proj. Rep. 20*, Geneva, Switzerland.

Zanis, P., et al. (2003), Forecast, observation and modelling of a deep stratospheric intrusion event over Europe, *Atmos. Chem. Phys.*, *3*, 763–777.